

Functional Imaging of Tendon

A. K. Harvey^{1,4}, M. S. Thompson¹, L. E. Cochlin², P. A. Raju¹, Z. Cui¹, H. R. Cornell³, P. A. Hulley³ and Sir M. Brady¹

¹Department of Engineering Science, University of Oxford, Oxford, UK

²Department of Physiology, Anatomy and Genetics, University of Oxford, Oxford, UK

³Botnar Research Centre, Nuffield Department of Orthopaedics, Rheumatology, and Musculoskeletal Sciences, Headington, Oxford, UK

⁴Life Sciences Interface Doctoral Training Centre, University of Oxford, Oxford, UK
(harvey@robots.ox.ac.uk)

Abstract

Tendons are composed of cells, blood vessels and extracellular matrix, intricately woven together to form a vital musculoskeletal connective tissue. They act as a mechanical buffer for transmitting forces generated in muscles to bones, thus enabling movement. There is a growing need for functional imaging of tendon, for example to provide non-invasive biochemical and biomechanical insight into injured, diseased or repairing tendon. This study focuses on *ex vivo* imaging using a novel combination of state of the art imaging technology, specifically ultra-high field magnetic resonance imaging (MRI) and near infrared-multiphoton laser scanning microscopy (NIR-MPLSM). We show that both imaging modalities are able to distinguish between normal and damaged tendon. MR imaging revealed macroscopic changes and evidence of tissue disruption; high signal intensity corresponding to surrounding sheaths and some intra-tendinous regions. NIR-MPLSM demonstrated that local interactions between collagen and other matrix components are altered in enzyme-digested tendon. We propose a novel method for quantifying tendon disruption based on tendon crimp waveform parameterisation. Our findings suggest that MRI and NIR-MPLSM are useful technologies for extracting functional information from tendon. We provide insight into how biomechanical properties are related to biochemical parameters, and thus consider the future of *in vivo* functional MR imaging of tendon.

1 Introduction

Tendon is a type of connective tissue which connects muscle to bone, constituting a vital component of the musculoskeletal system, by enabling movement. Tendons suffer from a wide range of disorders, including different mechanical injuries and degenerative diseases. Consequently, there is a growing demand for *in vivo* methods to functionally explore tendon in injury and disease, and monitor the tissue during subsequent healing and repair.

Current clinical assessment of tendon is predominantly subjective and symptomatic, although non-invasive imaging techniques such as elastography and ultrasound are becoming more widespread as functional tools. The major limitation of ultrasound, however, is that it is limited to tendon tissue which is superficial. Elastography, on the other hand, requires external mechanical or vibrational stimulation. The full potential of magnetic resonance imaging (MRI), in providing functional insight into tendon tissue, has scarcely been realised. This is perhaps because the MR signal intensity from tendons acquired using most clinical protocols is low, so much so that tendons appear as dark bands, making it difficult to extract any physiologically meaningful information. In order to enhance understanding of tendon MRI, it is necessary to investigate the underlying physiological properties of the tissue, and determine functionally relevant parameters.

The three dimensional and hierarchical (Figure 1) organisation of tendon make it possible for large forces from muscle to be transmitted to bone, without damaging the macroscopic tendon. From collagen monomers through fibrils, fibres and fascicles, the interactions between collagen (65-80% dry weight), cells, and other extracellular matrix (ECM) proteins at different levels of the hierarchy govern the functional properties of tendon. The ECM provides structural support for cells, occupies the intracellular space and helps provide mechanical support by buffering tensile and compressive tissue strains. Despite the small percentage of ECM occupied by proteoglycans (PGs) (0.2-5.0% dry weight), these proteins can hold water about 50 times their weight due to their negatively charged, hydrophilic, polysaccharide glycosaminoglycan (GAG) side-chains Kannus [2000]. For example, chondroitin sulphate (CS) is an abundant tendon GAG involved in regulating fibrillogenesis (fibril formation and development), fibril diameter, and cell proliferation Yoon and Halper [2005].

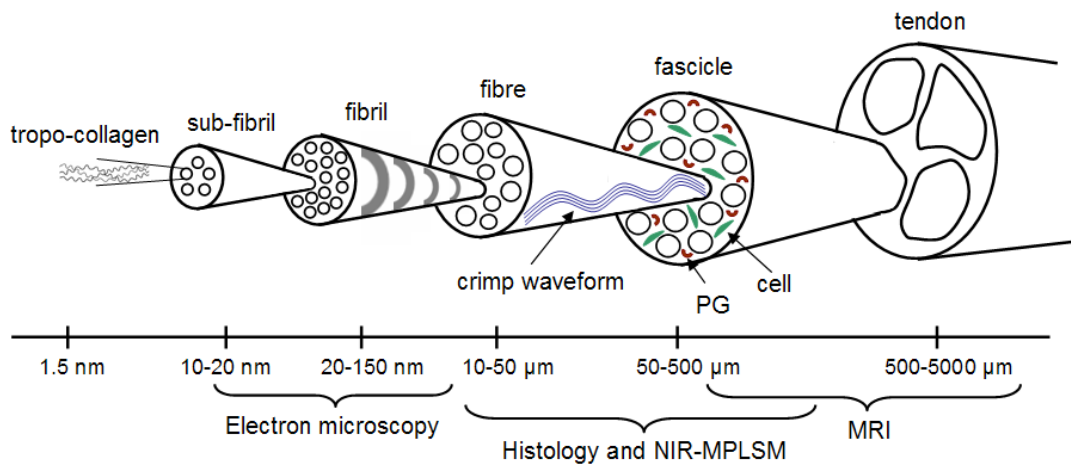


Figure 1: Tendon structure at different levels of the tendon hierarchy, and scale-appropriate imaging modalities. The crimp waveform is shown at the fibre level.

An important morphological feature of tendon tissue associated with mechanical properties is the regular repeating crimp of the collagen Diamant *et al.* [1972], which can be observed as a periodic banding of dark lines at the fibre level (Figure 1). It has been demonstrated that the crimp pattern is stretched out under strain Franchi *et al.* [2007], and that it can act as a shock absorber Diamant *et al.* [1972]. Crimping is typically demonstrated by polarised light microscopy, but is also visible using near infrared-multiphoton laser scan-

ning microscopy (NIR-MPLSM). NIR-MPLSM can generate three dimensional image stacks similar to confocal microscopy, and additionally has the capability of second harmonic generation (SHG). SHG is an endogenous nonlinear excitation process which occurs upon coincident absorption of two NIR photons in structures such as collagen. Since SHG does not involve excitation of molecules, it should in principle not suffer from phototoxicity or photo bleaching effects.

The abundance of collagen I makes tendon an excellent candidate for SHG. Since SHG images represent collagen structure, they provide intrinsic information about the fibre geometry and crimping waveform. Methods for quantifying crimp morphology can therefore provide parameters relating to tissue function. To our knowledge, the only crimp parameter which has so far been quantified for assessing tendon function is the crimp angle Franchi *et al.* [2007]. We however propose that SHG images contain information for characterising crimp in terms of tissue geometry, which can be related to the quality of the tissue. Specifically, the crimp waveform and curvature may be important biomarkers for normal and damaged (or degenerated) tendons. Such analysis can provide a framework for studying the interactions between the ultrastructure and ECM proteins of tendon.

The spatial interactions between collagen and other ECM proteins, such as GAGs, are important for determining tendon biomechanical properties Screen *et al.* [2005], and these spatial interactions can also be visualised using NIR-MPLSM. Moreover, the ECM high negative fixed charge density (FCD), dominated by GAGs, has an interesting property which can be exploited using a relatively novel MRI approach: FCD quantification for estimating cartilage degradation, by examining the distribution of a charged gadolinium-based contrast agent (CA) within the ECM Bashir *et al.* [1996]. Since tendon has similar ECM composites to cartilage, this FCD hypothesis could be exploited in tendon imaging. Using imaging techniques to localise biochemical microstructures, it is therefore possible to extract biomechanical information from images, providing a rigorous interpretation framework and valid underpinning assumptions.

This study is focussed on functional imaging of *ex vivo* tendon tissue, and is aimed at providing a physiological understanding of the signals produced by ultra-high field MRI and NIR-MPLSM. Firstly, we apply MRI and NIR-MPLSM to visualise normal tendon cells, blood vessels, collagen, surrounding sheaths and ECM components. We validate the imaging techniques using well established histology techniques and demonstrate that quantitative analysis of NIR-MPLSM images enables estimation of parameters relating to tendon function. We propose a novel method for detecting and quantifying the crimp waveform shape and curvature. Secondly, we investigated the potential of MRI to assess tissue quality, by comparing MRI and NIR-MPLSM of normal and enzyme-digested tendon, and quantifying their crimp morphology. Finally, we discuss the clinical implication of our result in the context of a novel non-invasive MRI method for assessing tendon tissue quality.

2 Materials and Methods

2.1 Normal Tendon

Extracted adult bovine lower limb tendons ($N = 10$) were cut into homogenous samples of length, ~ 10 mm, and diameter, ~ 5 mm. Image acquisitions were performed along transverse and longitudinal axes using MRI and NIR-MPLSM. Well established histological stain-

ing techniques were used to validate the MRI and NIR-MPLSM imaging. NIR-MPLSM images were quantified to estimate functionally relevant ECM parameters relating to crimp.

Ultra-High Field Magnetic Resonance Imaging. Samples were incubated in gadolinium (Gd)-based MRI contrast agent (CA) or phosphate buffered saline (PBS) for 16 hours at 37°C. Tendon samples were immobilised in agarose gel within a perspex specimen holder, specifically designed for MR imaging of *ex vivo* samples. MR imaging was carried out using a 300 MHz horizontal bore 7 Tesla magnet interfaced to a Varian Inova console (Varian Inc., Palo Alto, CA) using a transmit receive quadrature birdcage coil (55 mm) diameter at 20°C. T₂-weighted imaging was performed using a fast spin echo sequence with a repetition time (TR) of 0.3 s and an echo spacing (TE) of 0.015 s. T₁-weighted imaging was performed using a fast spin echo sequence with TR 0.1 s and TE 0.0125 s.

Near Infrared-Multiphoton Laser Scanning Microscopy. A NIR-MPLSM system Mulholland and Kendall [2003] was employed to image SHG from fibrillar collagen Theodossiou *et al.* [2006] in tendon. The system consists of a diode pumped Ti:Sapphire crystal laser (Mira-Coherent, Ely, UK) that provides 150 fs pulses of NIR light, coupled to a BioRad Radiance 2100 MPD laser-scanning system (Carl Zeiss GmbH, Germany) and a Nikon E600 FN upright microscope (Nikon UK Ltd, Surrey, UK). For SHG acquisition, laser excitation was conducted at 800 nm and emissions were captured by the filter corresponding to blue light (400 – 430 nm). Image stacks were acquired with a z-stack separation of 0.45 μm . LaserSharp software (Carl Zeiss, Hertfordshire, UK), provided online control of the system for image acquisition. Sections were stained via one of two protocols:

1. Texas red-wheat germ agglutinin (100 $\mu\text{g}/\text{ml}$ TR-WGA, Molecular Probes) for non-specific staining of lectins (polysaccharide) and cells.
2. Immunohistochemistry (IHC) for visualising chondroitin sulphate (CS) GAG in the ECM. Primary and secondary antibodies used were CS-56 (Sigma, dilution 1:100 in PBS) and AlexaFluor-488 (Invitrogen, dilution 1:100 in PBS), respectively.

AlexaFluor-488 and TR-WGA fluorescence emissions were captured by the channel setups corresponding to green (500 – 530 nm) and red (610 – 650 nm) light.

Histology. Histological staining was used to validate MRI and NIR-MPLSM imaging techniques. Sections were stained with Safranin-Orange (Safranin-O) and Alcian Blue (Nuclear Fast Red counter-stain), both of which are cationic and bind to GAG polyanions. Sections were viewed using a transmission light microscope.

Quantification of ECM Parameters. ImarisTM 5.0 (Bitplane AG) software Bitplane AG [2008] was used to: quantify ECM volumes; segment cells (seeded region-growing algorithm with estimated cell diameter of 20 μm) Shapiro and Stockman [2001]; calculate cell density and sphericity; and calculate co-localisation.

Custom-written routines in MATLAB R2008b were used to estimate crimp waveform parameters relating to intrinsic fibre geometry captured by the SHG images. Firstly, Canny edge detection was performed (see Canny [1986] for details), followed by spline curve fitting.

Splines, S , were fitted to edges comprising more than 20 connected pixels ($m > 20$):

$$S(x) = \sum_{i=1}^m P_i \bar{k}_i(x) \quad : \quad m > 20, \quad (1)$$

where the control points, P_i , are defined by the Canny edge co-ordinates. For each spline curve fitted in the image, waveforms were defined as peak-to-peak (local maxima) and trough-to-trough (local minima) regions of the spline. Each crimp waveform was then parameterised by estimating: crimp waveform amplitude, A ; wavelength, λ ; and curvature, κ . The curvature, deviation from a straight line, was estimated using the Frenet-Serret equations do Carmo [1976], a differential geometry technique.

2.2 Enzyme-Digested Tendon

Tendon samples were incubated in PBS, or enzyme-containing buffer (papain, trypsin, collagenase) for 16 hours at 37°C. Samples were imaged using the ultra-high field MRI and NIR-MPLSM immunohistochemical protocols described above. For NIR-MPLSM, three regions ($n = 3$) of each normal and enzyme-digested sample were imaged. The SHG images were quantified by estimating the crimp waveform parameters: wavelength, λ , amplitude, A , and curvature, κ . Within each region, the spline-fitting algorithm detected between 130–230 waveforms. Significant differences between the normal and enzyme-digested treatments were determined using one-way analysis of variance (ANOVA), at the 5 % significance level.

3 Results

3.1 Normal Tendon

Ultra-High Field Magnetic Resonance Imaging and Histology. Tendon MR images, contrast enhanced (CE)-MR images and corresponding histologically stained sections are shown in Figure 2. Incubation in CA clearly enhances the tendon signal (Figures 2A and E compared to H and I). The surrounding epitenon sheath in the transverse MRI slice (Figures 2A and H) appears bright, which can be attributed to fat, known to have a high MR signal intensity. The intra-tendinous signal may represent biochemical components of the ECM or paratenon, another fatty and fascicular sheath. Histological staining shows fascicular bundling (Figures 2B and C) and epitenon blood vessels (Figures 2B and D). Figure 2E shows the asymmetric setting of the surrounding sheath in agarose gel. Longitudinal fibre directionality and integrity can be identified in the MR images (Figures 2E and I), and are confirmed by the histologically stained sections (Figures 2F and G).

Near Infrared-Multiphoton Laser Scanning Microscopy and Histology. NIR-MPLSM images of normal tendon samples stained with TR-WGA and corresponding histologically stained sections stained with Alcian Blue and Safranin-O are presented in Figure 3. Emissions from collagen (Figure 3A), polysaccharide residues (Figure 3B) and tendon cells (Figure 3D) are captured in the blue, red and green channels, respectively. The merged image (Figure 3E) shows relative spatial locations of ECM microstructures. Elongated tendon cells are aligned along and between the collagen fibres, and the pericellular matrix is richer in

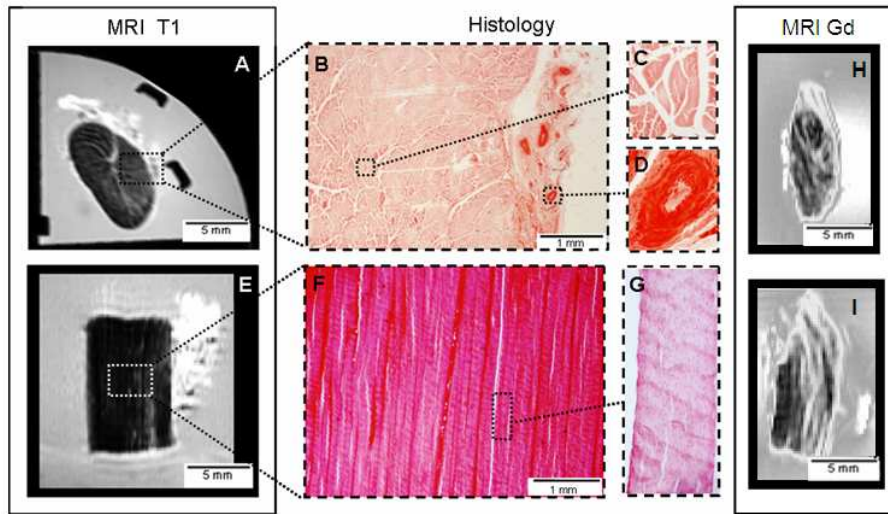


Figure 2: Tendon MR images (A and E), CE-MR images (H and I) and anatomically corresponding histologically stained sections stained with Safranin-O (B, C, D, F and G). Transverse slice revealing surrounding sheath, blood vessels and fascicular bundles (top row). Longitudinal slice showing fibre directionality and integrity (bottom row). Gd - gadolinium.

polysaccharide residues than other ECM regions. Histological staining confirmed the presence of cells and GAG at the relevant concentrations (Figures 3C and F), thus validating this type of NIR-MPLSM investigation of tendon tissue.

Quantification of ECM Parameters. Three dimensional reconstruction of NIR-MPLSM image stacks enabled volume quantification of different biochemical components: collagen I ($\sim 6,535,000 \mu\text{m}^3$), polysaccharide residues ($\sim 3,538,000 \mu\text{m}^3$), and tendon cells ($\sim 314,000 \mu\text{m}^3$). Tendon cells (Figure 4A) were segmented (Figure 4B) and quantified: tendon cell number per section (398), cell density ($\sim 44,000 / \text{mm}^3$), and sphericity (mean = 0.75) (Figure 4C). Co-localisation of blue (Figure 4D) and red (Figure 4E) channels reveals the spatial interactions between collagen and polysaccharide residues (Figure 4F). Collagen (Figure 4G), polysaccharide residues (Figure 4H) and tendon cell (Figure 4I) images are merged with the co-localisation result. Cells do not appear outside the co-localisation channel.

Normal tendon crimp quantification showed average waveform parameters of: amplitude, $A = 5.12$; wavelength, $\lambda = 32.9$; and curvature, $\kappa = 0.0405$. These results are presented in Table 1 compared to the enzyme-digested tendon results.

3.2 Enzyme-Digested Tendon

MRI and corresponding NIR-MPLSM images of PBS-incubated and enzyme-digested tendon samples are shown in Figure 5. MRI can identify macroscopic changes to the tendon: PBS-treated tendon reveals normal fibre directionality (Figure 5A); papain and trypsin induced moderate damage captured by MRI (Figures 5B and C); and collagenase-digestion caused severe identifiable damage, with little or no intact structure remaining (Figures 5D).

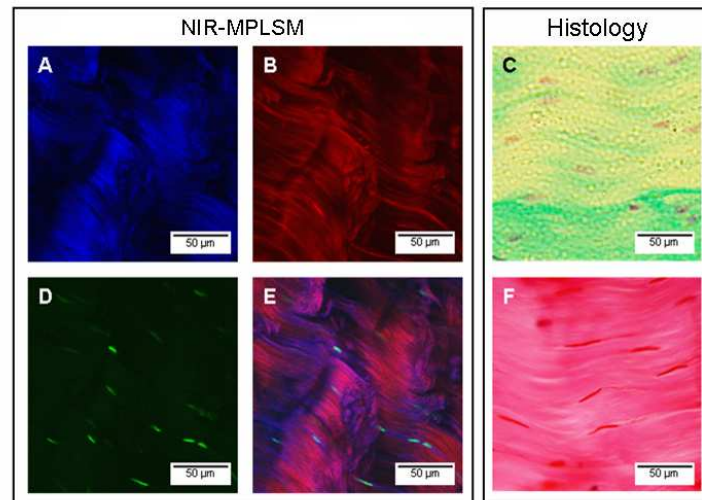


Figure 3: Tendon NIR-MPLSM images stained with TR-WGA and corresponding histologically stained sections. Images of collagen (A), polysaccharide residues (B) and cells (C) are merged (D) to show their relative spatial locations. With Alcian Blue and Nuclear Fast Red staining, tendon cells appear red, and GAGs are stained blue (C). Safranin-O stains the tendon cells dark pink, and the ECM a GAG concentration-dependent pink intensity (F).

NIR-MPLSM of tendon samples stained via the IHC protocol reveal that the signals corresponding to collagen (Figures 5E-H) and CS GAG (Figures 5I-L) are altered by enzyme-digestion. Merged images (Figures 5M-P) show that enzyme digestion reduces the amount of CS GAG present between the collagen fibres, and in particular trypsin allowed only vascular CS GAG to remain intact. Qualitatively, papain (Figure 5F) and collagenase (Figure 5H) appear to alter the crimp waveform, while trypsin-induced damage seems to manifest between the fibre bundles. (Figure 5H).

Spline curves fitted to the crimp waveform using the edge detection method are shown superimposed onto the SHG images (Figures 5O-T). Quantifiable parameters (A , λ and κ) for the normal and enzyme-digested SHG images are shown in Table 1. Overall, the crimp amplitude and curvature were reduced in the digested samples compared to the normal tendon sample. Crimp wavelength remained the same or increased after digestion, which would be expected if the amplitude is reduced. Significant differences between crimp parameters of normal and enzyme-digested tendon are denoted by * at the 5 % significance level: papain and collagenase digestion significantly reduced the crimp amplitude; and papain also significantly reduced the curvature (Table 1).

4 Discussion

This study shows for the first time that MRI and NIR-MPLSM can reveal functional information relating to normal and enzyme-digested tendon on corresponding tendon samples. Intra-tendinous signal was attained using ultra-high field MRI, and future CE-MRI work will further enhance understanding of contrast more rigorously. MRI was able to distin-

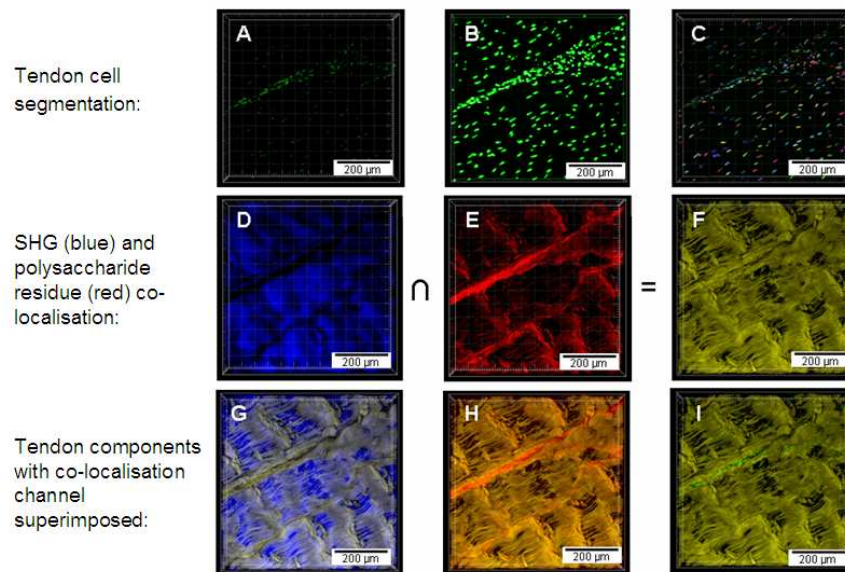


Figure 4: Quantification of TR-WGA stained NIR-MPLSM images. Tendon cells (A), result of region-growing algorithm (B) and segmentation result (C). Collagen in the blue (D) and polysaccharide residues in the red channel (E) are co-localised in the yellow channel (F). Co-localisation result merged with collagen (G), polysaccharides (H) and tendon cell (I) images.

guish between normal and damaged tendon at a macroscopic scale, with the changes in signal intensity likely being related to the underlying biochemistry of the ECM. Histological and NIR-MPLSM imaging clearly distinguished cells, blood vessels, collagen and ECM components. Specific probing of CS GAG alongside collagen-induced SHG revealed differences in normal and enzyme-digested tendon samples.

SHG images were quantified within a framework based on crimp waveform morphology, known to be functionally important in tendon Franchi *et al.* [2007]. Quantifiable ECM changes, such as reduced crimp waveform amplitude and curvature, could be attributed to breaking of collagen cross-links or reduction in CS GAG induced by enzyme-digestion. Our findings imply that NIR-MPLSM and MRI are potential tools for assessing clinical diseased, injured or repairing tendon. Imaging human normal and damaged tendon both *ex vivo* and *in vivo* using our imaging methods are important areas for future work.

Although histological and NIR-MPLSM images can provide similar information at high magnifications, a major benefit of the NIR-MPLSM system is that image stacks can be reconstructed in three dimensions, an important consideration for examining the biomechanical properties and interactions within the tissue. Another benefit of using an NIR-MPLSM system is that specific excitation of fibrillar collagen generates endogenous SH signals, thus requiring no stain and reflecting intrinsic tissue geometries. Intact vasculature is important for tendon health and repair, and the geometry of the blood vessels can influence the MR signal, for example in the administration of intravenous CA. Therefore, the demonstration of blood vessels in the epitenon and intra-tendinous compartments are vital consideration for future MRI work, with major implications for *in vivo* functional imaging of tendon.

The presented combination of state of the art imaging techniques across imaging modal-

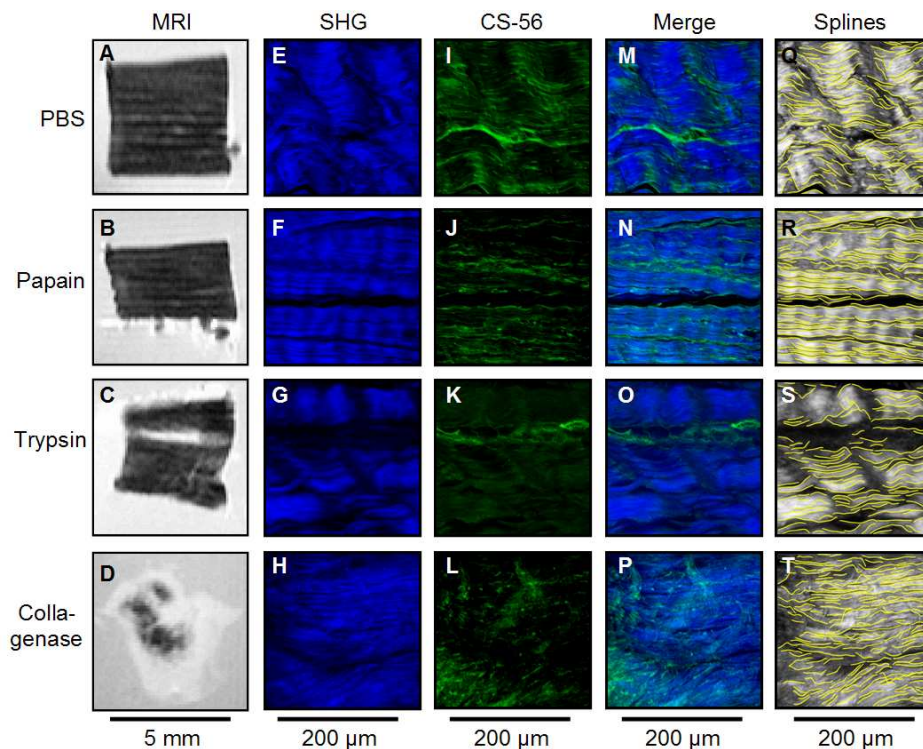


Figure 5: Normal and enzyme-digested tendon MRI (A-D) and NIR-MPLSM images (E-P). Both imaging modalities are able to detect enzyme-induced damage. Spline curves superimposed on the SHG images (O-T).

ities, matrix biology and image analysis has presented a unique opportunity for functional investigation of tendon tissue, enabling assessment of tissue quality, with potential for translation to an *in vivo* imaging tool.

5 Conclusions

Our findings have demonstrated novel imaging techniques for functionally exploring tendon tissue. Both MRI and NIR-MPLSM were able to distinguish between normal and enzyme-digested tendon at a microscopic level. SHG images were quantified using a novel method based on crimp waveform detection, an important mechanical parameter. Collagen and GAG spatial distributions is another important physiological parameter known to be linked to tendon biomechanical properties Screen et al. [2005]. Further downstream, this concept will enable exploration of non-invasive *in vivo* MR-based functional imaging tools for clinically assessing tendon injury, disease and repair.

Acknowledgements

The authors would like to thank Uday Tirlapur and Clarence Yapp for their contributions in NIR-MPLSM image acquisition, and Anthony McIntyre for his help with MRI. A. K. Harvey

Enzyme Incubation	A (μm)	λ (μm)	κ
PBS (normal)	5.12 ± 1.87	32.9 ± 4.11	0.0404 ± 0.000596
Papain	$2.77 \pm 0.280^*$	42.9 ± 5.68	$0.0266 \pm 0.00660^*$
Trypsin	3.57 ± 1.05	33.2 ± 9.97	0.0378 ± 0.00115
Collagenase	$2.76 \pm 0.416^*$	32.7 ± 3.26	0.0347 ± 0.00550

Table 1: Quantification (mean values \pm standard deviation) of crimp parameters for normal and enzyme-digested samples. Significant differences between crimp parameters after PBS- and enzyme-treatment, as tested by one-way ANOVA analysis, are denoted by * at 5 % significance level. A is amplitude; λ is wavelength; and κ is curvature.

is funded by the EPSRC-led Life Sciences Interface Doctoral Training Centre. P. A. Hulley is funded by Arthritis Research Campaign and RCUK Fellowships.

References

- A. Bashir, M. L. Gray, and D. Burstein. Gd-DTPA²⁻ as a measure of cartilage degradation. *Magnetic Resonance in Medicine*, 36(5):665–673, 1996.
- ImarisTM 5.0 Bitplane AG. Personal communication with Luciano Lucas, Oxford, 2008.
- J. Canny. A computational approach to edge detection. *IEEE PAMI*, 8(6):679–698, 1986.
- J. Diamant, A. Keller, E. Baer, M. Litt, and R. G. Arridge. Collagen; ultrastructure and its relation to mechanical properties as a function of ageing. *Proc R Soc Lond B Biol Sci*, 180(60):293–315, 1972.
- Manfredo P. do Carmo. *Differential Geometry of Curves and Surfaces*. Prentice Hall, New Jersey, 1976.
- M. Franchi, M. Fini, M. Quaranta, V. De Pasquale, M. Raspanti, G. Giavaresi, V. Ottani, and A. Ruggeri. Crimp morphology in relaxed and stretched rat achilles tendon. *J Anat*, 210(1):1–7, 2007.
- P. Kannus. Structure of the tendon connective tissue. *Scandinavian Journal of Medicine and Science in Sports*, 10(6):312–320, 2000.
- W. J. Mulholland and M. A. F. Kendall. Design and commissioning of a directly coupled in-vivo multiphoton microscope for skin imaging in humans and large animals. In *SPIE conference on Microscopy and Optical Design*, St Etienne, France, 2003.
- H. R. C. Screen, J. C. Shelton, V. H. Chhaya, M. V. Kayser, D. L. Bader, and D. A. Lee. The influence of noncollagenous matrix components on the micromechanical environment of tendon fascicles. *Annals of Biomedical Engineering*, 33(8):1090–1099, 2005.
- L. G. Shapiro and Geroge C. Stockman. In *Computer Vision*, pages 279–325. Prentice-Hall, New Jersey, 2001.

- T. A. Theodossiou, C. Thrasivoulou, C. Ekwobi, and D. L. Becker. Second harmonic generation confocal microscopy of collagen type i from rat tendon cryosections. *Biophys J*, 91(12): 4665–77, 2006.
- J. H. Yoon and J. Halper. Tendon proteoglycans: biochemistry and function. *Journal of Musculoskeletal Neuronal Interaction*, 5(1):22–34, 2005.